A TEST RIG FOR MEASURING FORCE AND TORQUE PRODUCTION IN A LORENTZ, SLOTLESS SELF BEARING MOTOR

Barrett A. Steele, Research Assistant
University of Kentucky, Bearings and Seals Laboratory, Lexington, Kentucky,
barrett_steele@hotmail.com
Lyndon S. Stephens, Assistant Professor
University of Kentucky, Bearings and Seals Laboratory, Lexington, Kentucky,
stephens@engr.uky.edu

ABSTRACT

An option to hybrid Maxwell/Lorentz type self bearing motors and their inherent trade-off between bearing force and motoring torque with PM magnet thickness is one which utilizes Lorentz forces for bearing and motoring force production. A slotless version of this type of self bearing motor, and its test rig, are discussed in this paper. The test rig includes the motor, along with a conventional magnetic bearing, a shaft assembly, radial position sensors and an optical encoder. Experimental results are presented showing the force versus current relation for the self bearing motor and indicates that several of the destabilizing side pull forces predicted by theory may be neglected in practice. In particular, the cross coupled bearing current gain for the motor is experimentally shown to be negligible as compared to the direct bearing current gain. This result provides the basis for stabilizing control of the motor. The current gain for the torque production was measured as 2.5 N-m/A, and that for bearing force production was measured as 48.2 N/A. These results are shown to agree well with theory.

INTRODUCTION

Self bearing motors combine magnetic bearing and torque production into a single actuator. This is desirable because of the resulting reduction in the overall length of a motor's shaft and because mechanical bearings need not be used. As a consequence, a shortened shaft length and elimination of additional bearings results in a shaft weight reduction. This twofold effect increases the system's natural frequencies and decreases the possibility of experiencing rotordynamic vibration problems.

Several investigators have recently studied permanent magnet self bearing motors [1], [2], [3], [4]. For the motors in studies such as these, the bearing forces are Maxwell-type forces that act between the rotor and the stator. Lorentz-type forces acting between the rotor and current carrying conductors provide the motoring torque. A problem with these designs is that to increase torque, one must increase the permanent magnet (PM) thickness. In doing so, however, the bearing force is reduced because of increased path reluctance through the thicker magnets. Slotted designs came about to optimize this design. These slotted designs, while successful, naturally include significant detent and cogging torque because of the preferred positioning of the rotor's permanent magnets and the stator's teeth. For precision-pointing applications, this design characteristic is debilitating and, therefore, very undesirable.

An alternative to the hybrid reluctance/Lorentz type designs is introduced by Stephens [5]. It is termed the Lorentz type, slotless self bearing motor. In this design, Lorentz type forces are used to produce both the bearing forces and the motoring torque, resulting in an actuator where thicker PM's result in larger torque production and larger force production. This essentially eliminates the trade-off in bearing force and motoring torque with PM thickness found in many previous designs. Further the design is slotless so detent and cogging torque is minimized, making this actuator well suited as a servo motor for precision pointing applications. The Lorentz, slotless design has also been studied on the basis of fault tolerance in a companion paper to this one [6].

This paper describes an experimental test rig designed to measure the open loop and closed loop properties of the Lorentz type, slotless self bearing motor proposed in [5]. Both the feedback loop and mechanical portion of the experimental rig are described. Experimental procedures for measuring the open loop current gains and position stiffnesses are detailed. Finally, experimental results are presented and compared to those predicted by theory. Good agreement is seen between the experimental and theoretical results, both qualitatively and quantitatively. These measurements provide the basis for future work focused on stabilizing the self bearing motor.

FORCE AND TORQUE GENERATION IN THE SLOTLESS, LORENTZ SELF BEARING MOTOR

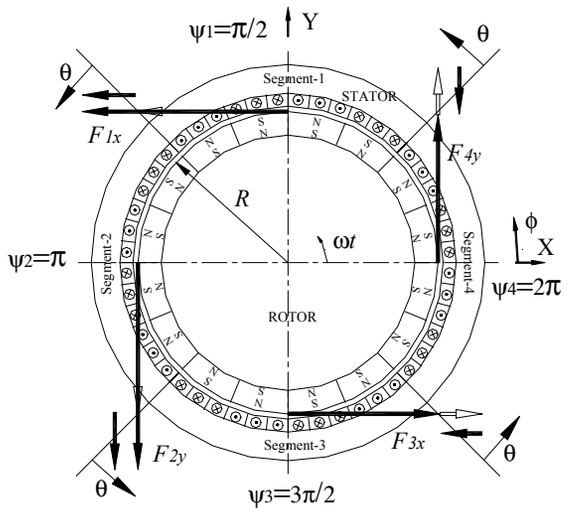

FIGURE 1: Actuator Layout and Force Generation Principle

Figure 1 illustrates the layout of the self bearing motor, and shows the Lorentz type force vectors required to rotate and center the rotor. The motor consists of M=8 PM pole pairs on the rotor and N_{seg}=4 individually controlled winding segments attached to a slotless stator. Each winding segment is an arc of π/2 radians. The windings in each segment are 3 phase with a 60 degree commutation angle, and occupy N_s=12 winding stations with N_w=85 wires per station. Each segment produces a traction on the surface of the rotor. Each traction is resolved into the segment forces, F_{1x}, F_{2y}, F_{3x} and F_{4y}, by proper construction of the motor. These forces can be used to produce motoring torque, and modulated to produce controllable bearing forces in the x and y directions. The following mapping between the segment currents, $i_1 - i_4$, and the directional control currents, i_x, i_y and i_θ is used:

$$\begin{aligned} i_1 &= (i_\theta - i_x) \\ i_2 &= (i_\theta - i_y) \\ i_3 &= (i_\theta + i_x) \\ i_4 &= (i_\theta + i_y) \end{aligned} \qquad (1)$$

Using this current mapping and assuming ideally sinusoidal PM flux and winding current distributions about the motor circumference, [5] shows that the force and torque generated by the motor are approximated, for small rotor eccentricities, by equations of the form:

$$F_x = K_b i_x + K_{pm} x - K_L i_\theta y + (K_{cr} + K_w i_\theta) i_y \qquad (2)$$

$$F_y = K_b i_y + K_{pm} y + K_L i_\theta x - (K_{cr} + K_w i_\theta) i_x \qquad (3)$$

$$T_\theta = K_{i\theta} i_\theta \qquad (4)$$

where the two control gains K_b, and $K_{i\theta}$ govern the bearing control forces and torque production, and the gains K_{pm}, K_L, K_{cr} and K_w are destabilizing. The control gains are approximated for all rotor angular positions, ωt, by:

$$K_b = \varepsilon \sqrt{2} L B_m N_w N_s \qquad (5)$$

$$K_{i\theta} = \varepsilon \pi L R B_m N_w N_s \qquad (6)$$

where L is the motor length, B_m is the maximum value of the sinusoidal PM flux distribution, R is the rotor radius and ε=cos(Mγ) is a correction factor that accounts for the pole pair number, M, and the phase difference, γ, between the PM flux distribution and the winding current distribution. K_b varies slightly with angular position of the rotor. Figure 2a illustrates this variation for the 8 PM pole pair motor where $\overline{K}_b = K_b/(1.414\varepsilon L B_m N_w N_s)$. Figure 2a indicates that this variation is negligible.

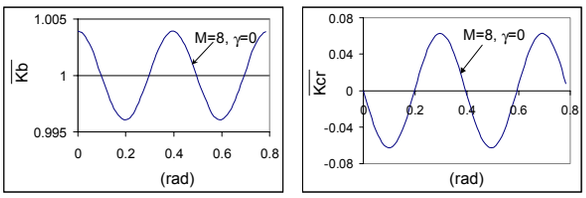

(a) (b)

FIGURE 2: Variation in Force Constants

K_{pm} is the negative stiffness due to the PM flux interacting with the stator and is analogous to the negative stiffness in a typical magnetic bearing. K_{pm} is computed as:

$$K_{pm} = \frac{\pi R L B_r^2 t_m^2 \mu_R K_{ml} C_\phi}{2\mu_o [t_m + \mu_R K_{ml} C_\phi (g_o + t_c)]^3} \qquad (7)$$

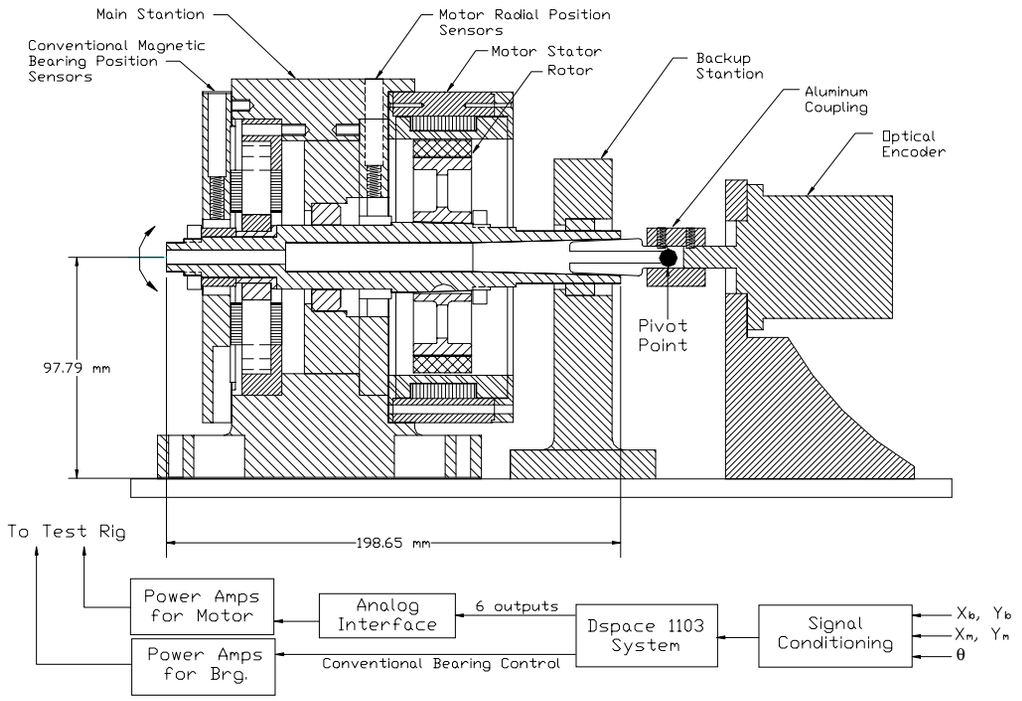

FIGURE 3: Experimental Test Rig for Self Bearing Motor

where B_r is the remnance flux, t_m is the PM radial thickness, t_c is the radial thickness of the windings, g_o is the nominal radial air gap, μ_o is the permeability of free space, μ_R is the recoil permeability, K_{ml} the magnet to magnet leakage factor and C_ϕ is the flux concentration factor. K_L is the cross-coupled position stiffness that results due to Lorentz interactions between the PM flux and the winding currents when the shaft is in the eccentric position. K_L is computed by:

$$K_L = \frac{\varepsilon \pi B_r \mu_R K_{ml} C_\phi L t_m N_w N_s}{2[t_m + \mu_R K_{ml} C_\phi (g_o + t_c)]^2} \tag{8}$$

K_{cr} is the cross-coupled current gain resulting from Lorentz interactions even when the shaft is in the centered position. Like K_b, K_{cr} varies with rotor angular position. Figure 2b illustrates this variation about zero where $\overline{K}_{cr}=K_{cr}/(1.414\varepsilon L B_m N_w N_s)$. As Figure 2 indicates, $\overline{K}_{cr,mx} << K_b$, which is necessary in order to produce independent bearing forces and torque in the motor.

Finally, K_w is the cross coupled current gain resulting in a reluctance (Maxwell) type side pull force due to a non-symmetric winding flux interacting with the rotor. The non-symmetric winding flux occurs even when the rotor is in the centered position and is non-zero only when large torque and bearing forces are required, simultaneously. K_w is approximated by:

$$K_W = \frac{\sqrt{2}\mu_o R L \left[N_w \left(2N_s / M \right) \right]^2}{(t_m + t_c + g_o)^2} \tag{9}$$

For a thorough derivation of these gains and a description of the control algorithm of the motor the reader is referred to references [5] and [6]. In the next section, an experimental test rig, that is used to measure certain effects of the force and torque gains, is described.

TEST RIG DESCRIPTION

A table top test rig was constructed for the self bearing motor and is shown in Figure 3. The rig consists of a conventional 8-pole magnetic bearing on the outboard end of a shaft (outboard is the end furthest from the encoder) with inductive probes measuring radial displacements, X_b and Y_b. The slotless self bearing motor is assembled near the mid span of the shaft and uses inductive probes to measure the radial displacements X_m and Y_m. Using two different sets of position probes reduces the susceptibility of the system to sensor-actuator noncollocation problems. The other end of the shaft is connected to a rotary optical encoder providing the angular measurement, θ. The connection uses a Jarno interface and an aluminum coupling such that the encoder ball bearings support one end of the shaft through the coupling, while the other end of the shaft is free to move radially, pivoting about the coupling as illustrated in the figure. In order to stabilize the shaft, either the

conventional magnetic bearing or the self bearing motor can be used. In addition, the conventional magnetic bearing can be used as a force sensor to measure the force characteristics of the self bearing motor.

TABLE 1: Summary of Test Rig Construction

	Property	Symbol	Units	Value
Motor Properties	Number of Pole Pairs	M	--	8
	Number of Segments	N_{seg}	--	4
	Number of Winding Stations per Segment	N_s	--	12
	Number of Wires per Winding Station	N_w	--	85
	Radial Thickness of Permanent Magnets	t_m	*(mm)*	7.75
	Radial Thickness of coil windings	t_c	*(mm)*	3.87
	Nominal radial air gap	g_o	*(mm)*	0.762
	Rotor Outer Radius	R	*(mm)*	50.8
	Motor Length	L	*(mm)*	25.4
System Properties	Distance from Pivot Point to External Load	L_x	*(cm)*	19.9
	Distance from Pivot Point to Mag. Bearing	L_b	*(cm)*	15.9
	Distance from Pivot Point to Motor	L_m	*(cm)*	7.75
	Control Bandwidth	BW	*(Hz)*	3,000
	Controller Hardware	dSPACE DS1103 Card		
	Power Amplifiers	Advanced Motion Controls		

The feedback loop of the system consists of the five sensor measurements, $X_b, Y_b, X_m, Y_m, \theta$ that are conditioned and fed into a dSPACE DS1103 motion control system. The control algorithm is detailed in [5] and [6], and produces a set of control current requests for the conventional magnetic bearing and for the self bearing motor. The self bearing motor's control loop utilizes an additional analog stage in formulating the four 3 phase segment currents. A group of 16 Advanced Motion Control power amplifiers then generate the self bearing motor and the conventional magnetic bearing control currents.

The shaft assembly is shown in detail in Figure 4, along with the first three free-free flexible modeshapes. The shaft is designed to have the fewest possible flexible body modes within the control bandwidth of 3 kHz. The shaft assembly consists of a sensor target for the conventional magnetic bearing, a stack of thin laminated journals for the conventional magnetic bearing, a sensor target for the motor bearing and the self bearing motor rotor with permanent magnets attached. The stator housing and encoder stanchion are mounted on a common baseplate. The shaft assembly is quite stiff with the first three shaft flexible modes at 2,792 Hz, 5,625 Hz and 9,271 Hz. Only the first flexible mode is within the control bandwidth of 3 kHz, which is limited by the power amplifiers. Table 1 summarizes the construction of the test rig and the self bearing motor.

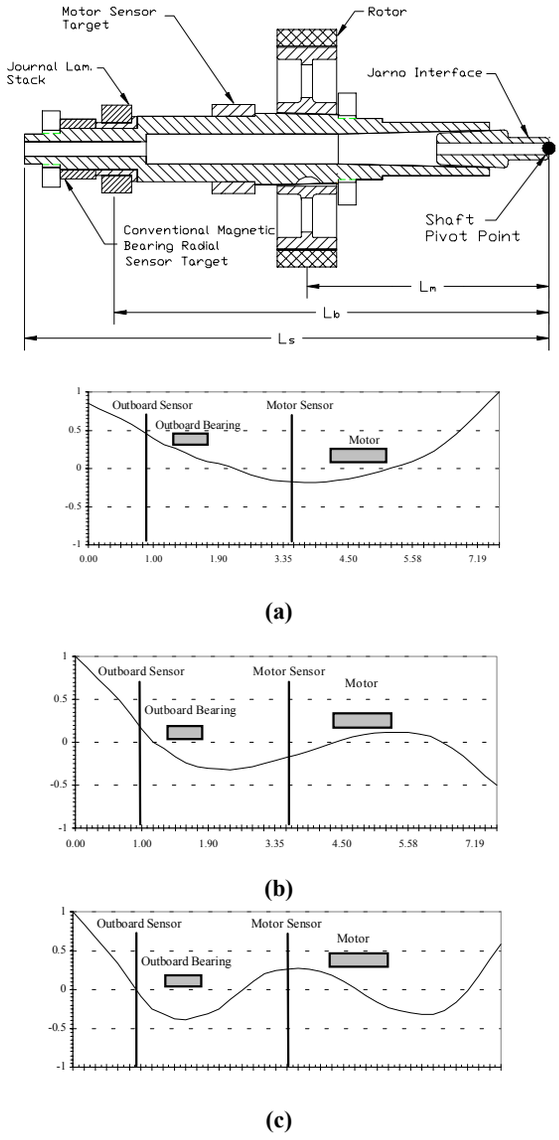

FIGURE 4: Shaft's First Three Flexible Body Modes (a) 2792 Hz, (b) 5625 Hz, (c) 9271 Hz

Figure 4 also shows the location of each sensor plane, the self bearing motor and the conventional magnetic bearing. Comparing the location of these components to the vibration nodes in each mode shape gives an indication of any controllability, observability and non-collocation problems. The first mode is quite observable and controllable from the sensor and actuator locations, and it does not suffer from sensor actuator non-collocation.

EXPERIMENTAL

Force Measuring Procedures

As mentioned previously, one function of the conventional magnetic bearing in the test rig is to act as a force sensor for the self bearing motor. This is done by determining the static closed loop force versus displacement relationship for the magnetic bearing using the following procedure. The magnetic bearing is located a distance of L_b=15.9 cm from the pivot point (see Figure 4). It is stabilized under PD control; therefore, it resists applied loads statically just as a mechanical spring does. Known loads are then applied to the shaft at the outboard end, a distance of L_s=19.9 cm from the pivot point, and the displacement is measured at the magnetic bearing plane. Using the previously calibrated displacement sensitivity of the radial position sensor, S_{sensor}=8.4 V/mm, and scaling the results by the appropriate lever arms from the pivot point (L_s and L_b), a force vs. displacement curve is generated. Figure 5 shows the resulting calibration curve for the bearing x-direction which results in a static force sensitivity (the closed loop bearing stiffness) of S_{force}=532 N/mm. Note that this includes the side pull force of the PM rotor as it was in place on the shaft during calibration. Finally, this calibration curve is used for both the x and y direction forces as these axes are symmetric.

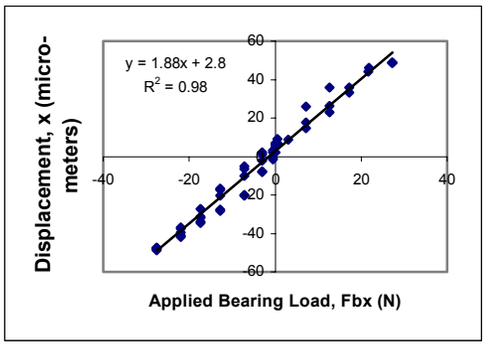

FIGURE 5: Magnetic Bearing Calibration Curve

The force generation characteristics of the self bearing motor are measured using the static force sensitivity of the conventional magnetic bearing, S_{force}, and the following procedure. First, the angular positioning loop for the motor is closed, resulting in a torsional position stiffness, which maintains the same angular position during testing. Open loop bearing forces are then generated by the self bearing motor using the control currents, i_x and i_y. These open loop forces act on the shaft at the motor, a distance of L_m=7.75 cm from the pivot point. The displacement at the magnetic bearing is then measured and the static force sensitivity used to compute the open loop force applied by the motor. This procedure is used in the following section to measure the force generation of the self bearing motor.

Results and Discussion

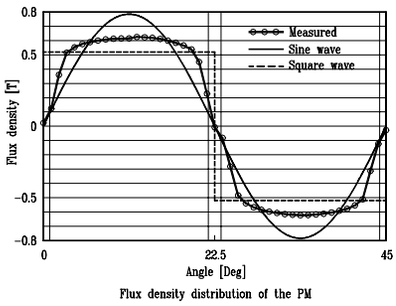

FIGURE 6: PM Flux Density Distribution

Figure 6 shows a plot of the measured PM flux density at different points along the face of one of eight identical pole pairs while the rotor is centered inside the stator. The plot also includes a fitted square wave and the ideal sine wave. Note that the theoretical actuator properties in equations (5)-(9) are based on the sine wave approximation. B_m = 0.8 T is used in these equations to compute the theoretical results. The difference between the ideal sine wave and the measured PM flux distribution is a source of error between the measured and theoretical results.

TABLE 2: Measured and Theoretical Results, γ=0

Property	Symbol	$\phi = 0^0$	$\phi = 11.25^0$
		Theory/ Measured	Theory/ Measured
Torque Gain	$K_{i\theta}$ (N-m/A)	3.4/ 2.5	3.4/ 2.5
Bearing Force Current Gain	K_b (N/A)	29.3/ 48.2	29.3/ 53.3
Cross Coupled Bearing Force Gain, max.	K_{CR} (N/A)	0/ 1.7	1.8/ 3.2
Negative Stiffness Due to PMs	K_{PM} (N/A)	43,570/ --	43,570/ --
Position Stiffness Due to Lorentz Forces	K_L (N/m*A)	3,496/ --	3,496/ --
Side Pull Due to Winding Flux	K_W (N/A^2)	0.97/ --	0.97/ --

Table 2 summarizes the theoretical and experimental actuator gains for the self bearing motor. The open loop torque gain was measured using a simple torque wrench and found to be 2.5 N-m/A, which compares well with the theoretical value of 3.4 N-m/A. To measure the open loop bearing forces in the motor, the feedback loop in the angular direction, θ, is closed using a PID controller. With no torsional load applied to the motor during testing, the control current was measured as i_θ = 0.050 A. For this value of i_θ, the side pull forces due to K_L and K_W

are computed as 0.006 N and at 0.005 N, respectively, based on equations (8) and (9). Therefore, these terms are assumed to be negligible in the experimental force measurement. Further, since the calibration curve of Figure 5 includes the effects of K_{PM}, the side pull force will not be measured by this procedure. This leaves only two terms in the bearing force equations: the direct and the cross-coupled bearing force gains, which are of the most interest since they relate to i_x and i_y, which are used to control the system.

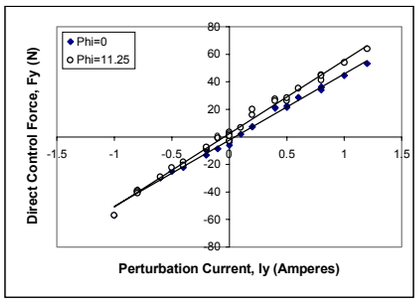

(a)

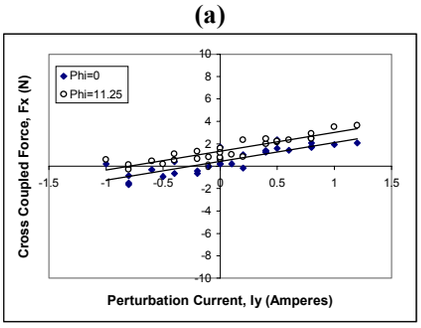

(b)

FIGURE 7: Force Variation with Control Current, i_y

Figure 7 shows the variation in the x and y-direction forces with the control current, i_y, at two rotor angular positions of 0^o and 11.25^o. Referring to Figure 2, these rotor positions correspond to the average and peak values of K_b and K_{cr}, respectively. The direct bearing current gain, K_b, is the slope of the lines in Figure 7a, and is measured as 48.2 N/A and 53.3 N/A at 0^o and 11.25^o, respectively. These compare to theoretical values of 29.3 N/A for both positions. The main difference between the theoretical and experimental results is most likely due to the actual flux distribution being closer to a square wave than a sine wave as shown in Figure 5. The cross-coupled bearing current gain, K_{cr}, is the slope of the lines in Figure 7b, and is found to be 1.7 N/A and 3.2 N/A at 0^o and 11.25^o, respectively. These compare to a theoretical value of zero and 1.8 N/A at each position.

The most significant experimental result is that $K_{cr} << K_b$, which confirms the theoretical results found in [5]. Specifically, the theoretical results show that $K_{cr,max}$ is 6.1% of K_b, and the experimental results show that $K_{cr,max}$ is 6.6% of K_b. Therefore, the cross coupled term can be considered negligible as compared to the direct term and independent bearing force in each direction are practically, if not strictly, generated. This provides the basis for stabilizing control of the self bearing motor.

SUMMARY AND CONCLUSIONS

This paper described the force and torque generation principles of the Lorentz self bearing motor. A test rig was also described that can be used to measure the force and torque constants of the motor. Experimental results were presented showing the force versus current relation for the self bearing motor, and indicating that several of the destabilizing side pull forces predicted by theory may be negligible in practice. In particular, the cross coupled bearing current gain for the motor was experimentally shown to be negligible as compared to the direct bearing current gain. This result provides the basis for stabilizing control of the motor.

ACKNOWLEDGEMENTS

The authors express their appreciation to Airex Corporation of Dover, N.H., U.S.A., and to the United States Air Force for their sponsorship of this research under contract F04701-97-C-0014. They also wish to thank Kathy Hardesty for her assistance in conducting experimental research for this project.

REFERENCES

[1] J. Bischel, "The bearingless electrical machine," in *Proc. Int. Symp. Magn. Suspension Technol.'91,* NASA Publication 3152, Langley Research Center, Hampton, VA, pp. 561-573, August, 1991.

[2] A. Chiba, M.A. Rahman, and T. Fukao, "Radial forces in bearingless reluctance motor," *IEEE Trans. Magnetics,* vol. 27, p. 786, Mar. 1991.

[3] R. Schoeb and J. Bichel, "Vector control of bearingless motor," in *Proc. 4th Int. Symp. Magn. Bearings,* ETH Zurich, Switzerland, pp. 327-332, 1994.

[4] Y. Okada, S. Miyamoto, and T. Ohishi, "Levitation and torque control of internal permanent magnet type bearingless motor," *IEEE Trans. Control Syst. Techn.,* vol. 4, no. 5, pp. 565-571, 1996.

[5] L.S. Stephens and D. Kim, "Analysis and simulation of a Lorentz-type slotless, self-bearing motor," *Proc. Of 1st IFAC Conf. On Mechatronic Systems,* Sep. 2000.

[6] D. Kim and L.S. Stephens, "Fault tolerance of a Lorentz-type slotless, self-bearing motor according to the coiling schemes," in *Proc. 7th Int. Symp. Magn. Bearings*, ETH Zurich, Switzerland. August, 2000.